Asynchronous Uplink Sensors Fused in Perceptive Mobile Networks

Zhitong Ni[1,2], J. Andrew Zhang[2], Xiaojing Huang[2], and Kai Yang[1]
[1] Beijing Institute of Technology, School of Information and Electronics, China
[2] University of Technology Sydney, Global Big Data Technologies Centre (GBDTC), Australia
zhitong.ni@student.uts.edu.au; Andrew.Zhang@uts.edu.au; yangkai@bit.edu.cn.

***Abstract*—This paper proposes a scheme that solves two challenging problems in parameter estimation using communication signals: (1) asynchronous transmitter and receiver; and (2) sensing receiver with a small number of antennas. These problems exist in parameter estimation for perceptive mobile networks and WiFi. The geometrically-separated transmitter and receiver in communications are typically asynchronous at clock level. For a small base-station or WiFi, the number of antenna elements in an array is usually limited, which limits the resolution of estimating the angle-of-arrivals (AOAs) of multipath signals. In this paper, we employ cross-antenna cross-correlation (CACC) operation to resolve the asynchronous issue and use the CACC outputs to generate a multi-domain signal block that combines three-domain receive samples to efficiently increase the resolution of AOAs. The proposed scheme enables the direct use of uplink communication signals for radio sensing, without requiring any modifications on infrastructure or advanced hardware, such as a full-duplex transceiver. It also enables the estimation of more number of paths than the number of antennas, hence sensing in a small base-station or WiFi becomes possible.**

***Index Terms*—Joint communication and radar sensing, dual-functional radar-communications, uplink sensing, WiFi sensing**

I. Introduction

The emerging joint communication and radio sensing (J-CAS) techniques fuse communication and radio sensing functions into one system, sharing one single transmitted signal and many hardware and signal processing modules [1], [2]. The fusion achieves immediate benefits of reduced size, power consumption, cost, and improved spectrum efficiency [3], [4]. Moreover, the JCAS techniques can establish a communication link using sensing information or vise versa [5]. Evolving from the current communication-only mobile network, the JCAS-enabled mobile network is expected to serve as a ubiquitous radio-sensing network, whilst providing uncompromising mobile communication services [6]–[8]. Similar ideas have also been proposed to realize sensing in indoor WiFi systems [9], [10].

There exists an optional transceiver setup for realizing JCAS in mobile networks or WiFi, similar to a bi-static radar [11], where the sensing receiver is physically separated from the transmitter. Such a setup can be implemented requiring minimal changes and can be a favorite option in the near term. This setup is consistent with the uplink sensing as defined in [7], where transmitters and sensing receivers are physically separated. The main difficulties for using this setup are the clock-level asynchronism between the sensing receiver and the transmitter, and the relatively low angle-of-arrival (AOA) accuracy due to the small number of antennas. Perfect synchronization was assumed in [7], and the asynchrony between the sensing receiver and the transmitter is not addressed yet. The asynchrony will generally introduce timing offsets (TOs) and carrier frequency offsets (CFOs), resulting in ranging ambiguity and velocity ambiguity, respectively, during sensing.

There have been a limited number of works on passive WiFi sensing that handle asynchronous transceivers based on a cross-antenna cross-correlation (CACC) method [9], [10], [12]. The underlying principle of CACC is that TOs and CFOs across multiple antennas in one device are the same, and hence can be removed by computing the cross-correlation between signals from multiple receiving antennas. In [10], CACC was applied to tackle the AOA estimation problem for device-free human tracking with commodity WiFi devices. In [9], CACC was used to resolve the ranging estimation problem for passive human tracking using a single WiFi link. CACC has the disadvantage of creating side products in the correlated signals. The author in [10] proposed an add-minus suppression (AMS) scheme to retrieve the parameters including delays and Doppler frequencies of targets. Their proposed method suppresses the side product and then conduct the cross correlation operations. The method can suppress the side product to some extent, but it is susceptible to the power distribution and the number of static and dynamic signals. In [13], the authors proposed a mirrored MUSIC method that can perfectly address the issues of side products. For these WiFi sensing schemes, we note that the relatively low accuracy of AOA estimates is not addressed yet. The main reason for the low AOA resolution is that the AOAs are obtained based on the estimates of delays and Doppler frequencies, that is, the accuracy of AOAs is dependent on that of delays and Doppler frequencies.

In this paper, we propose an uplink sensing scheme that can address the above-mentioned two issues, i.e., those offsets caused by the asynchronous setups and the dependent AOA estimations. We extend the CACC methods to mitigate the timing and frequency ambiguity. Then, using the CACC outputs, we stack received signals into a multi-domain signal block that contains all three parameters, including the delays, Doppler frequencies, and AOAs of targets. Via MUSIC estimators, we can estimate these parameters without including

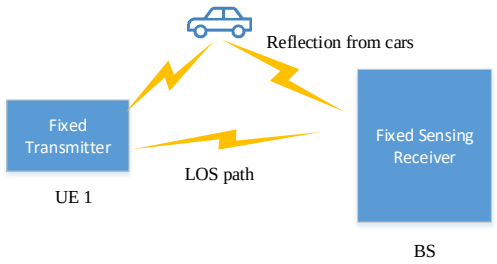

Fig. 1. Basic system setup.

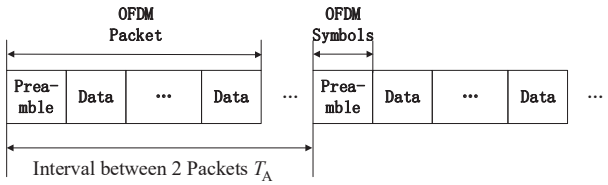

Fig. 2. Illustration of transmitted OFDM packets at the UE baseband.

any approximation. The multi-domain signal block enlarges the dimension of the spatial domain and hence increases the accuracy of AOA estimates.

Notations: $\mathbf{a}$ denotes a vector, $\mathbf{A}$ denotes a matrix, italic English letters like N and lower-case Greek letters α are a scalar, $\angle a$ is the phase angle of complex value a. $|\mathbf{A}|, \mathbf{A}^T, \mathbf{A}^H, \mathbf{A}^\dagger$ represent determinant value, transpose, conjugate transpose, pseudo inverse, respectively. We denote Frobenius norm of a matrix as $\|\mathbf{A}\|_F$. We use $\mathrm{diag}(\alpha_1, \cdots, \alpha_k)$ to denote a diagonal matrix. $[\mathbf{A}]_N$ is the Nth column of a matrix and $[\mathbf{A}]^N$ is the Nth row of a matrix.

II. System Model and Related Solution

A. System Model

We consider the sensing scenario in a small base-station (BS). The same setup can also be applied to other applications, such as the one in WiFi sensing [9]. During sensing, multiple user equipments (UEs) communicate with the BS. The BS is physically static and uses received uplink signals for both communication and sensing. Each UE has one antenna and the BS has a limited number of N antennas. Our proposed scheme in this paper requires two assumptions for the system setups: 1) The communication signals used for sensing are transmitted from a specific UE, denoted as UE 1, of which location is fixed and known to the BS; 2) There is a LOS propagation path between the BS and the UE 1, and the power of the LOS path is much larger than that of non-LOS (NLOS) paths.

The fixed UE can be a node that provides fixed broadband access in the mobile network. We can adopt a high-frequency band to guarantee the dominating power of the LOS path. The required setups are practically feasible that can be applied to many kinds of communication system structures, such as WiFi systems and mobile networks. In this work, we use the proposed scheme for sensing the targets in a small BS. Without loss of generality, we consider sensing via the uplink signal from the UE 1. We assume synchronization is not achieved between the UE 1 and the BS.

At all UEs, we adopt the same packet structure, as shown in Fig. 2. In each packet, training symbols, denoted as preambles, are followed by a sequence of data symbols. Orthogonal-frequency-division-multiplexing (OFDM) modulation is applied across the whole packet. In this paper, we only use the preambles for sensing multiple targets. The parameters of targets including the propagation delay, Doppler frequency, and AOA need to be obtained. Without losing generality, we assume each packet has only one preamble.

For both preamble symbol and data symbol, each of them is an OFDM symbol that has G subcarriers with a subcarrier interval of $1/T$, where T denotes the length of an OFDM symbol. Each OFDM symbol is prepended by a cyclic prefix (CP) of period T_{C}. When multiple UEs communicate with the BS, each UE occupies a unique segment of subcarriers with the interleaved interval as in [14]. For notational simplicity, we assume that UE 1 occupies the whole preamble symbol here. Mathematically, the transmitted preamble symbol in the mth OFDM packet can be expressed as [15], [16]

$$s(t|m) = \sum_{g=0}^{G-1} \exp\left(j2\pi g \frac{t}{T}\right) \mathrm{rect}\left(\frac{t}{T+T_{\mathrm{C}}}\right) x[m,g], \quad (1)$$

where $x[m,g]$ is a modulated symbol transmitted on the gth subcarrier of the mth preamble symbol and $\mathrm{rect}\left(\frac{t}{T+T_{\mathrm{C}}}\right)$ denotes a rectangular window of length $T+T_{\mathrm{C}}$. We assume that M packets are sent at the same interval, denoted as T_{A}, at the UE baseband, as shown in Fig. 2.

The BS receives the preambles using a uniform linear array (ULA) of N antennas. The uplink channel between receiver at BS and the transmitter at UE 1 has L NLOS paths reflected or refracted from L targets, together with a dominating LOS path, where the index of the LOS path is denoted as $l = 0$. Let α_l, $f_{\mathrm{D},l}$, τ_l and θ_l denote the channel gain, the Doppler frequency, the propagation delay, and the AOA of the lth path, respectively. Due to the fixed locations of BS and UE 1, we assume that the parameters, τ_0 and θ_0, which correspond to the LOS path, are known at the BS, and $f_{\mathrm{D},0}$ is 0. We also assume that $|\alpha_0| \gg |\alpha_l|, \forall l \in \{1, \cdots, L\}$. Note that $f_{\mathrm{D},l}$ from the lth target of the channel can be either positive or negative depending on the moving directions.

Since there is typically no synchronization at clock level between the BS and the UE 1, the received signal has an unknown time-varying TO, denoted as $\delta_\tau(m)$, associated with the clock asynchrony, even if the packet level synchronization is achieved. Hence, the total time delay during signal propagation for the lth target as seen by the BS equals $\tau_l + \delta_\tau(m)$. In [9], it is shown that there also exists an unknown time-varying CFO due to the asynchronous carrier frequency, denoted as $\delta_f(m)$. The received time-domain $N \times 1$ signal vector corresponding to the mth preamble symbol can be

represented as [9]

$$\begin{aligned}\mathbf{y}(t|m) =& \sum_{l=0}^{L} \alpha_l e^{j2\pi m(T_{\rm A}+\delta_\tau(m)+\tau_l)(f_{{\rm D},l}+\delta_f(m))}\times \\ & s(t-\tau_l-\delta_\tau(m))\mathbf{a}(\Omega_l)+\mathbf{z}(t|m) \\ \approx& \sum_{l=0}^{L} \alpha_l e^{j2\pi m T_{\rm A}(f_{{\rm D},l}+\delta_f(m))}\times \\ & s(t-\tau_l-\delta_\tau(m))\mathbf{a}(\Omega_l)+\mathbf{z}(t|m), \end{aligned} \tag{2}$$

where the vector, $\mathbf{a}(\Omega_l)=\exp[j\Omega_l(0,1,\cdots,N-1)]^T$, is the array response vector of size $N\times 1$, with Ω_l being $\frac{2\pi d}{\lambda}\cos\theta_l$, d denoting the antenna interval, λ denoting the wavelength, and θ_l being the AOA from the lth target, and $\mathbf{z}(t|m)$ is a complex additive-white-Gaussian-noise (AWGN) vector with zero mean and variance of σ^2. TO is typically time-varying and has a random value that changes during any two discontinuous transmissions. The CFO may slowly vary over time. It is noted that TO and CFO are mixed with the actual propagation delay and the actual Doppler frequency, respectively. Hence, they can directly cause ambiguity of ranging and velocity measurements. The total delay and total Doppler frequency also vary with time due to these offsets. We use the approximation $e^{j2\pi m(T_{\rm A}+\delta_\tau(m)+\tau_l)(f_{{\rm D},l}+\delta_f(m))}\approx e^{j2\pi m T_{\rm A}(f_{{\rm D},l}+\delta_f(m))}$, since the timing values of $(\delta_\tau(m)+\tau_l)$ are much smaller than $T_{\rm A}$ and $(f_{{\rm D},l}+\delta_f(m))$ is also small compared to the sampling rate. It should be highlighted that, for the communication purpose, there is no need to distinguish the actual parameters of targets with these offsets, since they can be estimated as a whole value and then be removed. As for the purpose of sensing, these offsets have to be mitigated since the range and the velocity of targets only depend on actual parameters.

After removing CP from the received time-domain signal, we transform the signal into frequency domain via G-point fast-Fourier-transform (FFT)'s at the BS. Referring to (2), the received frequency-domain signal is

$$\begin{aligned} y'_n[m,g] =& \sum_{l=0}^{L} \alpha_l e^{jn\Omega_l} e^{j2\pi m T_{\rm A}(f_{{\rm D},l}+\delta_f(m))}\times \\ & e^{-j2\pi\frac{g}{T}(\tau_l+\delta_\tau(m))}x[m,g]+z'_n[m,g], \end{aligned} \tag{3}$$

where $y'_n[m,g]$ is the received frequency-domain signal on the gth subcarrier at the nth receiving antenna of the mth OFDM preamble symbol, and $z'_n[m,g]$ is a complex AWGN with zero mean and variance of σ^2. Since $x[m,g]$ is a known value to the BS, we divide $y'_n[m,g]$ of (3) by $x[m,g]$, i.e.,

$$y_n[m,g]=\frac{y'_n[m,g]}{x[m,g]}. \tag{4}$$

III. Proposed Signal Processing Scheme

As we mentioned in the section II, the actual delays and Doppler frequencies are mixed with TOs and CFOs, respectively. In this section, we propose a high-resolution soft parameter estimation algorithm by combining measurements from spatial, temporal, and frequency domains. The proposed algorithm is particularly useful when the number of antennas is small. Hence, our scheme is quite appropriate for realizing sensing in small BSs or WiFi devices.

We use CACC to mitigate CFOs and TOs. Different from the AMS scheme [10], we directly execute CACC between the received signal of the nth antenna and that of the 0th antenna. With neglecting the noise term, the received signal can be given by $y_n[m,g]=D_n[m,g]+I_n[m,g]$, with $D_n[m,g]$ being the signal from the LOS path and $I_n[m,g]$ being the signal from the NLOS paths. They are given by

$$D_n[m,g]=\alpha_0 e^{jn\Omega_0} e^{j2\pi m T_{\rm A}(f_{{\rm D},0}+\delta_f(m))} e^{-j2\pi\frac{g}{T}(\tau_0+\delta_\tau(m))}, \tag{5}$$

and

$$I_n[m,g]=\sum_{l=1}^{L}\alpha_l e^{jn\Omega_l} e^{j2\pi m T_{\rm A}(f_{{\rm D},l}+\delta_f(m))} e^{-j2\pi\frac{g}{T}(\tau_l+\delta_\tau(m))}. \tag{6}$$

Note that α_0 is the path gain of LOS path and should be much larger than $\alpha_l, l\neq 0$. The CACC signal is then given by

$$\begin{aligned}\rho_n[m,g] &= y_n[m,g]y_0^H[m,g] \\ &\approx (D_n[m,g]+I_n[m,g])(D_n[m,g]+I_n[m,g])^H \\ &\triangleq \rho_n^{(1)}+\rho_n^{(2)}[m,g]+\rho_n^{(3)}[m,g]+\rho_n^{(4)}[m,g], \end{aligned} \tag{7}$$

where $\rho_n^{(1)}=D_n[m,g]D_0^H[m,g]$, $\rho_n^{(2)}[m,g]=I_n[m,g]I_0^H[m,g]$, $\rho_n^{(3)}[m,g]=D_n[m,g]I_0^H[m,g]$, and $\rho_n^{(4)}[m,g]=I_n[m,g]D_0^H[m,g]$.

Then we obtain the high-pass component by using a high-pass filter over m and g. A simple high-pass filter can be realized by removing the mean value of $\rho_n[m,g]$, denoted as $\bar{\rho}_n$. The output from the high-pass filter is

$$\begin{aligned}\hat{\xi}_n[m,g] =& \rho_n[m,g]-\bar{\rho}_n \\ \approx& \rho_n^{(3)}[m,g]+\rho_n^{(4)}[m,g] \\ =& \sum_{l=1}^{L}\alpha_0\alpha_l^H e^{j2\pi m T_{\rm A}(-f_{{\rm D},l})} e^{-j\frac{2\pi g}{T}(\tau_0-\tau_l)} e^{jn\Omega_0} \\ & + \sum_{l=1}^{L}\alpha_l\alpha_0^H e^{j2\pi m T_{\rm A} f_{{\rm D},l}} e^{-j\frac{2\pi g}{T}(\tau_l-\tau_0)} e^{jn\Omega_l} \\ \triangleq& \xi_n[m,g]. \end{aligned} \tag{8}$$

Note that our proposed scheme will use $\hat{\xi}_n[m,g]$ as inputs to estimate all parameters. Without the noise term, the approximation error only comes from the operation of the high-pass filter. We can prove that our proposed scheme has less input error compared with the AMS scheme. Due to the page limit, we only verify it via simulations, as shown in the section IV.

Now, we propose a novel signal processing scheme that estimates all three parameters using the CACC outputs. Collecting $\xi_n[m,g]$ over all antennas, we form a vector as

$$\begin{aligned}\mathbf{c}[m,g] =& [\xi_1[m,g],\cdots,\xi_{N-1}[m,g]]^T \\ =& \sum_{l=1}^{L}\alpha_0\alpha_l^H e^{j2\pi m T_{\rm A}(-f_{{\rm D},l})} e^{-j\frac{2\pi g}{T}(\tau_0-\tau_l)}\mathbf{a}(\Omega_0) \end{aligned}$$

$$+\sum_{l=1}^{L}\alpha_l\alpha_0^H e^{j2\pi m T_{\mathrm{A}} f_{\mathrm{D},l}} e^{-j\frac{2\pi g}{T}(\tau_l-\tau_0)}\mathbf{a}(\Omega_l)$$

$$\triangleq \sum_{l'=-L,l\neq 0}^{L} P_{l'} e^{j2\pi T_{\mathrm{A}} m \bar{f}_{\mathrm{D},l'}} e^{-j\frac{2\pi g}{T}\bar{\tau}_{l'}}\mathbf{a}(\Omega_{l'}), \quad (9)$$

where $\mathbf{a}(\Omega_{l'}) = \exp[j\Omega_{l'}(1,\cdots,N-1)]$ is the array response vector with dimension of $(N-1)\times 1$, $P_{l'}$ equals $\alpha_0\alpha_l^H$ and $\alpha_0^H\alpha_l^H$ for $l'>0$ and $l'<0$, respectively, $\bar{\tau}_{l'}$ equals $\tau_0-\tau_l$ and $\tau_l-\tau_0$ for $l'>0$ and $l'<0$, respectively, and $\bar{f}_{\mathrm{D},l'}$ equals $-f_{\mathrm{D},l}$ and $f_{\mathrm{D},l}$ for $l'>0$ and $l'<0$, respectively. Since estimating AOAs in the spatial domain only has not a satisfactory performance due to the small number of antennas, we aim to combine the spatial domain with other domains to enlarge the dimension of array response vectors. Using $\mathbf{c}[m,g]$, we generate a matrix that has an enlarged dimension of array response vectors, given by

$$\mathbf{C}'[m,g] = \begin{bmatrix} \mathbf{c}[m,g] & \mathbf{c}[m,g] \\ \mathbf{c}[m,g+1] & \mathbf{c}[m+1,g] \\ \vdots & \vdots \\ \mathbf{c}[m,g+C-1] & \mathbf{c}[m+C-1,g] \end{bmatrix}, \quad (10)$$

where $C, C\in\mathbb{N}$, satisfies $4L/(N-1) < C < \min(G-4L, M-4L)$. The dimension of $\mathbf{C}'[m,g]$ is $C(N-1)\times 2$. The first column of $\mathbf{C}'[m,g]$ is an enlarged vector corresponding to the spatial (angle) domain and the frequency (delay) domain. The second column is an enlarged vector corresponding to the spatial (angle) domain and the time (Doppler frequency) domain. It can be proved that the basis vectors for the first column of $\mathbf{C}'[m,g]$ are given by

$$\mathbf{c}_{l'}^1 = \begin{bmatrix} \mathbf{a}(\Omega_{l'})e^{-j0\frac{2\pi}{T}\bar{\tau}_{l'}} \\ \mathbf{a}(\Omega_{l'})e^{-j1\frac{2\pi}{T}\bar{\tau}_{l'}} \\ \vdots \\ \mathbf{a}(\Omega_{l'})e^{-j(C-1)\frac{2\pi}{T}\bar{\tau}_{l'}} \end{bmatrix}. \quad (11)$$

Likewise, the basis vectors for the second column of $\mathbf{C}'[m,g]$ are given by

$$\mathbf{c}_{l'}^2 = \begin{bmatrix} \mathbf{a}(\Omega_{l'})e^{j0\cdot 2\pi T_{\mathrm{A}}\bar{f}_{\mathrm{D},l'}} \\ \mathbf{a}(\Omega_{l'})e^{j2\pi T_{\mathrm{A}}\bar{f}_{\mathrm{D},l'}} \\ \vdots \\ \mathbf{a}(\Omega_{l'})e^{j2(C-1)\pi T_{\mathrm{A}}\bar{f}_{\mathrm{D},l'}} \end{bmatrix}. \quad (12)$$

From the expression of the basis vectors, we see that the dimension of the array response vector enlarges C times. Hence, the signal vector of (10) can increase the resolution in the spatial domain, which enables a small number of antennas to have much higher resolution for estimating AOAs.

We then stack $\mathbf{C}'[m,g]$ into a multi-domain signal matrix,

$$\mathbf{C} = [\mathbf{C}'[0,0], \mathbf{C}'[0,1], \cdots, \mathbf{C}'[0,D]], \quad (13)$$

where $D, D\in\mathbb{N}$, satisfies $C+D < \min(M,G)$. For the columns of $\mathbf{C}$, the basis vectors are given by $\mathbf{c}_{l'}^1$ and $\mathbf{c}_{l'}^2$, with $l'\in\{\pm 1,\cdots,\pm L\}$. Hence, the rank of $\mathbf{C}$ is $4L$.

The columns of $\mathbf{C}$ are related to all parameters. However, directly estimating all parameters from $\mathbf{C}$ would be very challenging. Therefore, we propose a soft estimation algorithm that estimates all three parameters (delays, Doppler frequencies, AOAs) within 3 steps.

1) Step 1: Note that the parameters corresponding to the LOS path are assumed to be known at the BS. We first solve the MUSIC-based problems below to obtain delays and Doppler frequencies, respectively.

$$\hat{\tau}_l = \mathrm{Peak}^{\bar{L}}\left(\frac{1}{\left\|[\mathbf{c}^1(\Omega_0,-\tau')]^H\bar{\mathbf{U}}_{\mathrm{C}}\right\|_F^2}\right), l\in\{1,\cdots,\bar{L}\}, \quad (14)$$

and

$$\hat{f}_l = \mathrm{Peak}^{\bar{L}}\left(\frac{1}{\left\|[\mathbf{c}^2(\Omega_0,-f')]^H\bar{\mathbf{U}}_{\mathrm{C}}\right\|_F^2}\right), l\in\{1,\cdots,\bar{L}\}, \quad (15)$$

where $\mathrm{Peak}^{\bar{L}}(\cdot)$ denotes the operation that takes $\bar{L}$ estimates corresponding to the $\bar{L}$ largest peak values of the function in the bracket, $\tau'\in(0,\pi)$ and $f'\in(-\pi,\pi)$ are the testing values, $\bar{\mathbf{U}}_{\mathrm{C}}$ is the null-space in the left singular matrix of $\mathbf{C}$, i.e., the columns from the $(4L+1)$th column to the $C(N-1)$th column of the left singular matrix, $\mathbf{c}^1(\Omega_0,-\tau')$ has the same expression with $\mathbf{c}_{l'}^1$ in (11), with letting $\Omega_{l'}$ and τ_l' be replaced by Ω_0 and the testing value, $-\tau'$, respectively. Likewise, $\mathbf{c}^2(\Omega_0,-f')$ has the same expression as $\mathbf{c}_{l'}^2$, with letting $\Omega_{l'}$ and $\bar{f}_{\mathrm{D},l'}$ be replaced by Ω_0 and the testing value, $-f'$, respectively. Note that we obtain $\bar{L}>L$ estimates for both delays and Doppler frequencies. We call these estimates to be soft estimates since they are not actual estimates corresponding to L targets. We obtain more than L soft estimates because some estimates may have multiple peaks in the problem above. The L actual parameters exist in those $\bar{L}$ estimates almost for sure.

2) Step 2: The soft estimates of delays and Doppler frequencies are not automatically matched to one target. Hence, we need to make a pair for each estimate of delay with each estimate of Doppler frequency. We call this processing to be pair matching. This process can also filter out the actual L pairs of estimates from $\bar{L}$ estimates.

Since Ω_0 is known to the sensing receiver (BS), we can utilize Ω_0 to do the pair matching. The soft estimates that are obtained from (14) and (15) are denoted as $\hat{\tau}_{l_y}$ and $\hat{f}_{\mathrm{D},l_x}$. Note that there are $\bar{L}^2$ possibilities of pair matching, i.e.,

$$(\hat{f}_{\mathrm{D},l_x},\hat{\tau}_{l_y}), l_x\in\{1,\cdots,\bar{L}\}, l_y\in\{1,\cdots,\bar{L}\}. \quad (16)$$

The actual pair of estimates should have the maximum combining gain in the following function that combines $\xi_n[m,g]$ as follows.

$$P_\xi(l_x,l_y)$$

$$= \sum_{m=0}^{M-1} \sum_{g=0}^{G-1} \sum_{n=0}^{N-1} \xi_n[m,g] e^{jm2\pi T_{\mathrm{A}} \hat{f}_{\mathrm{D},l_x} - jg\frac{2\pi g}{T}(\hat{\tau}_{l_y} - \tau_0) - jn\Omega_0}. \tag{17}$$

We can first select one out of $\bar{L}^2$ candidates that maximizes the absolute value of $P_\xi(l_x, l_y)$. Supposing that the selected index of the obtained pair is (l_{x_0}, l_{y_0}), we remove this pair from the set of candidates. Hence, one pair of Doppler frequency and delay is determined. After removing the pair of (l_{x_0}, l_{y_0}), the number of candidates is reduced to $(\bar{L}-1)^2$, i.e., $l_x \in \{1, \cdots, \bar{L}\}, l_x \notin \{\pm l_{x_0}\}$, $l_y \in \{1, \cdots, \bar{L}\}, l_y \notin \{l_{y_0}\}$. We then match the next pair of Doppler frequency and delay. Repeating the process L times, we can match the total L pairs of Doppler frequencies and delays.

3) Step 3: With delays and Doppler frequencies determined, only NLOS AOAs, $\Omega_l, l \in \{1, \cdots, L\}$, need to be estimated. We solve the problem below L times and obtain L AOA estimates,

$$\hat{\Omega}_l = \mathrm{Peak}^1 \left(\frac{1}{\left\| \left[\mathbf{c}^1(\Omega', \hat{\tau}_l - \tau_0), \mathbf{c}^2(\Omega', \hat{f}_{\mathrm{D},l}) \right]^H \bar{\mathbf{U}}_{\mathrm{C}} \right\|_F^2} \right), \quad l \in \{1, \cdots, L\}, \tag{18}$$

where $\Omega' \in (-\pi, \pi)$ is a testing value. For each pair of delay and Doppler frequency, we only obtain one estimate as the NLOS AOA estimate. Hence, there are L NLOS AOAs estimates obtained from (18).

IV. Simulation Results

In this section, we provide simulation results to validate the proposed scheme. The carrier frequency is 35 GHz. The number of OFDM-system subcarriers is $G = 256$. The frequency bandwidth is 128 MHz. Therefore, the OFDM symbol period T is 2 us and the CP period T_{C} is 0.4 us. The approximate interval between two packets, T_{A}, is 1 ms. We use the preamble OFDM symbols in $M = 128$ packets for sensing parameter estimation. The propagation delay is randomly distributed over $[0, 0.4]$ us, and the Doppler frequency is randomly distributed over $[-0.2, 0.2]$ KHz. Assume that the BS has a ULA with $N = 8$ antenna elements. Unless stating otherwise, we assume that there is one LOS path and $L = 3$ NLOS paths that are reflected or refracted from 3 targets. The power of the LOS path is 10 dB higher than those of the NLOS paths.

Fig. 3 presents the MSE of $\xi_n[m,g]$, defined as $|\hat{\xi}_n[m,g] - \xi_n[m,g]|^2$. The MSE of $\xi_n[m,g]$ reflects the accuracy of the constructed high-pass signals and directly impacts the following sensing parameter estimation. Two schemes are tested to filter out the low-pass component. One is our proposed scheme. The other one is the AMS scheme. For simplicity, we minus the mean value of $\xi_n[m,g]$ to realize the high-pass filter. It is clear that our proposed scheme outperforms the AMS scheme. It is worth pointing out that the MSE of our applied filter drops linearly with the SNR increasing for $L = 1$ target. This indicates that the input error of $\xi_n[m,g]$ can be sufficiently small when there is only one target. This is because, when $L = 1$, $\rho_n^{(2)}[m,g]$ is also a low-pass component, and when there are multiple targets, the MSE approaches to a fixed level that is the mean power of $\rho_n^{(2)}[m,g]$.

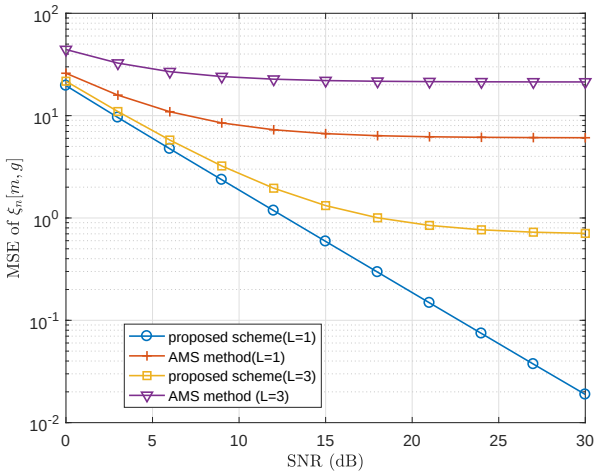

Fig. 3. MSE of $\xi_n[m,g]$ versus SNR and number of paths.

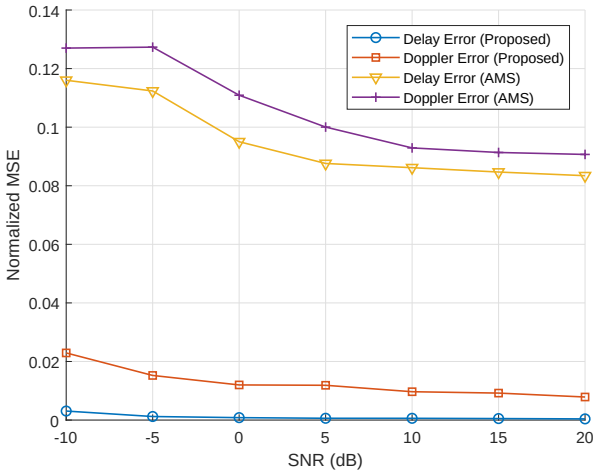

Fig. 4. NMSE of delays and Doppler frequencies versus SNR.

Fig. 4 illustrates the normalized MSE (NMSE) versus SNR for delays and Doppler frequencies. The bench-marking solution is the AMS method in [10]. For the initialization of our proposed soft estimation scheme, C is set to 60, D is 50, and $\bar{L}$ is 5, which meet their respective range requirement. At high SNRs, the NMSEs of delays and Doppler frequencies are quite satisfying, which are below 0.02. The error of Doppler frequency is larger than that of delay, which can be explained by the fact that there are more samples in the frequency domain than those in the time domain. We also see that our proposed scheme outperforms the AMS method greatly.

Fig. 5 shows the NMSE of AOAs versus SNR. We compare our proposed scheme with the AMS method and the spatial domain resolution that equals $\left(\frac{2\pi}{N}\right)^2$. It is clear that our

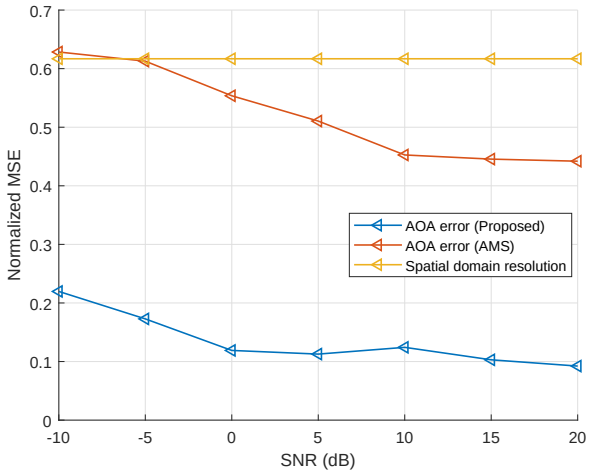

Fig. 5. NMSE of AOAs versus SNR.

achieved NMSE of AOAs outperforms the other two curves. For the spatial domain resolution, it is generally achieved by estimating AOAs in the spatial domain only. As for the AMS method, since the AOAs are obtained after obtaining the estimates of delays and Doppler frequencies, the error of AOAs is significantly larger than that of our proposed scheme. Their obtained AOA estimates depend on delays and Doppler frequencies. An error floor can be observed for our proposed scheme. This error floor could be caused by the error of the high-pass filter for obtaining $\xi_n[n, g]$. Compared with Fig. 4, the achieved AOAs have larger NMSE than delays and Doppler frequencies, which is mainly due to the fact that N is too small compared with M and G.

V. Conclusion

In this paper, we have proposed an uplink sensing scheme for small BSs or WiFi devices, which enables a communication system with asynchronous transceivers and a small number of antennas to realize JCAS functions. The proposed scheme efficiently handles the CACC outputs by generating a multi-domain signal block. Simulation results demonstrate that our proposed scheme can effectively estimate the actual values of delay, Doppler frequency, and AOA of targets. The results also show that the proposed uplink parameter estimation scheme outperforms the state of the arts and can accurately detect multiple targets in multiple sensing applications.

References

[1] C. Sturm and W. Wiesbeck, "Waveform design and signal processing aspects for fusion of wireless communications and radar sensing," *Proc. IEEE*, vol. 99, no. 7, pp. 1236–1259, Jul. 2011.

[2] A. R. Chiriyath, B. Paul, and D. W. Bliss, "Radar-communications convergence: Coexistence, cooperation, and co-design," *IEEE Trans. on Cogn. Commun. Netw.*, vol. 3, no. 1, pp. 1–12, Mar. 2017.

[3] J. A. Zhang, X. Huang, Y. J. Guo, J. Yuan, and R. W. Heath, "Multibeam for joint communication and radar sensing using steerable analog antenna arrays," *IEEE Trans. Veh. Technol.*, vol. 68, no. 1, pp. 671–685, Jan. 2019.

[4] Y. Luo, J. A. Zhang, X. Huang, W. Ni, and J. Pan, "Optimization and quantization of multibeam beamforming vector for joint communication and radio sensing," *IEEE Trans. Commun.*, vol. 67, no. 9, pp. 6468–6482, Sep. 2019.

[5] N. González-Prelcic, R. Méndez-Rial, and R. W. Heath, "Radar aided beam alignment in mmWave V2I communications supporting antenna diversity," in *2016 Information Theory and Applications Workshop (ITA)*, Jan. 2016, pp. 1–7.

[6] J. A. Zhang, A. Cantoni, X. Huang, Y. J. Guo, and R. W. Heath, "Framework for an innovative perceptive mobile network using joint communication and sensing," in *2017 IEEE 85th Vehicular Technology Conference (VTC Spring)*, Jun. 2017, pp. 1–5.

[7] M. L. Rahman, J. A. Zhang, X. Huang, Y. J. Guo, and R. W. Heath, "Framework for a perceptive mobile network using joint communication and radar sensing," *IEEE Trans. Aerosp. Electron. Syst.*, vol. 56, no. 3, pp. 1926–1941, Jun. 2020.

[8] M. L. Rahman, P. Cui, J. A. Zhang, X. Huang, Y. J. Guo, and Z. Lu, "Joint communication and radar sensing in 5G mobile network by compressive sensing," in *2019 19th International Symposium on Communications and Information Technologies (ISCIT)*, Sep. 2019, pp. 599–604.

[9] K. Qian, C. Wu, Y. Zhang, G. Zhang, Z. Yang, and Y. Liu, "Widar2.0: Passive human tracking with a single Wi-Fi link," in *Proceedings of the 16th Annual International Conference on Mobile Systems, Applications, and Services*. New York, NY, USA: Association for Computing Machinery, 2018, pp. 350–361. [Online]. Available: https://doi.org/10.1145/3210240.3210314

[10] X. Li, D. Zhang, Q. Lv, J. Xiong, S. Li, Y. Zhang, and H. Mei, "Indotrack: Device-free indoor human tracking with commodity Wi-Fi," *Proc. ACM Interact. Mob. Wearable Ubiquitous Technol.*, vol. 1, no. 3, Sep. 2017. [Online]. Available: https://doi.org/10.1145/3130940

[11] C. R. Berger, B. Demissie, J. Heckenbach, P. Willett, and S. Zhou, "Signal processing for passive radar using OFDM waveforms," *IEEE J. Sel. Topics Signal Process.*, vol. 4, no. 1, pp. 226–238, Feb. 2010.

[12] D. Garmatyuk, P. Giza, N. Condict, and S. Mudaliar, "Randomized OFDM waveforms for simultaneous radar operation and asynchronous covert communications," in *2018 IEEE Radar Conference (RadarConf18)*, 2018, pp. 0975–0980.

[13] Z. Ni, J. A. Zhang, X. Huang, K. Yang, and J. Yuan, "Uplink sensing in perceptive mobile networks with asynchronous transceivers," *IEEE Trans. Signal Process.*, vol. 69, pp. 1287–1300, 2021.

[14] Y. L. Sit, B. Nuss, and T. Zwick, "On mutual interference cancellation in a MIMO OFDM multiuser radar-communication network," *IEEE Trans. Veh. Technol.*, vol. 67, no. 4, pp. 3339–3348, Apr. 2018.

[15] J. Gu, J. Moghaddasi, and K. Wu, "Delay and Doppler shift estimation for OFDM-based radar-radio (RadCom) system," in *2015 IEEE International Wireless Symposium (IWS 2015)*, Mar. 2015, pp. 1–4.

[16] C. Sturm, Y. L. Sit, M. Braun, and T. Zwick, "Spectrally interleaved multi-carrier signals for radar network applications and multi-input multi-output radar," *IET Radar, Sonar Navigation*, vol. 7, no. 3, pp. 261–269, Mar. 2013.